Available online at www.sciencedirect.com
ScienceDirect
Polymer 49 (2008) 488–496
polymer
www.elsevier.com/locate/polymer

Polyethylene nanocomposites based on intercalation of *N*-alkyl amines within $KTiNbO_5$ structure

Sophie Chausson [a], Vincent Caignaert [a], Richard Retoux [a,*], Jean-Michel Rueff [a], Loïc Le Pluart [b,**], Pierre-Jean Madec [b], Paul-Alain Jaffrès [c]

[a] *CRISMAT, UMR CNRS 6508, ENSICAEN, Université de Caen Basse-Normandie, 6 Boulevard du Maréchal Juin, 14050 Caen, France*
[b] *Laboratoire de Chimie Moléculaire et Thio-organique, ENSICAEN, Université de Caen Basse-Normandie, CNRS, 6 Boulevard du Maréchal Juin, 14050 Caen, France*
[c] *UMR CNRS 6521, Faculté des Sciences et Techniques, Université de Bretagne Occidentale, 6 Avenue Le Gorgeu, 29238 Brest, France*

Received 24 August 2007; received in revised form 20 November 2007; accepted 22 November 2007
Available online 21 December 2007

Abstract

This article describes the synthesis of nanostructured organic/inorganic hybrid materials based on the modification of the titanoniobate oxide $KTiNbO_5$ by *N*-alkyl amines via an acido-basic reaction. X-ray diffraction and scanning electron microscopy have showed the successful intercalation of the organic molecules between the inorganic layers. The hybrid nanofillers previously obtained have been incorporated in a polyethylene matrix by melt intercalation. The morphology and thermomechanical properties of the nanocomposites have been investigated. It has been revealed that the modification of the oxide improves the dispersion and the exfoliation in the matrix leading to an increase of Young's modulus and of the degradation temperature. The TEM observations coupled with EDS mapping is revealed to be one interesting mean of characterization for this study.

Keywords: Nanocomposites; Hybrid layered materials; Titanoniobates

1. Introduction

Nanocomposites have received an amazing interest in the past two decades, not only in academic research but also in industrial world since 1989 when Toyota Central Research group published their research results on the physical property improvements of a nylon 6/clay nanocomposite [1–5].

From this time, much work has been focused on the influence of different types of nanofillers on various polymer matrixes, thermoplastic and thermoset. They demonstrated that the dispersion of a nanometer-scale inorganic filler at very low ratio in a polymer matrix can easily enhance a number of properties: thermal stability as well as mechanical and barrier properties [6,7].

One of the most largely studied nanofillers is layered silicates such as montmorillonite (MMT) [6–8]. The main advantages of these inorganic layers are low cost, a great potential specific area (more than 700 m^2/g), a high aspect ratio, a high cation exchange capacity (100 meq./100 g) and good swelling properties allowing intercalation of organic molecules in the interlayer space. Unfortunately, MMT has got several drawbacks: the dispersion of the polymer matrix is often incomplete; there is no full exfoliation but aggregation under tactoid form leading most of the time to an inhomogeneous material. These difficulties of dispersion lead to problems in understanding structure–property relationships of clay-based polymer nanocomposites and hence to contradictions in the literature [9–11]. This phenomenon is more emphasized for polyethylene nanocomposites for which the non-polarity of the matrix brings problems of compatibility and homogeneity

* Corresponding author. Tel.: +33 2 31451331; fax: +33 2 31951600.
** Corresponding author. Tel.: +33 2 31451386.
E-mail addresses: richard.retoux@ensicaen.fr (R. Retoux), loic.le_pluart@ensicaen.fr (L. Le Pluart).

0032-3861/$ - see front matter © 2007 Elsevier Ltd. All rights reserved.
doi:10.1016/j.polymer.2007.11.050

with different type of particles: TiO_2 [12], clay [10], carbon nanotubes [13].

We decided to study another category of layered nanofillers which has been only introduced in polymers by Bruzaud et al. [14,15]: $KTiNbO_5$. This mineral oxide was first prepared in 1962 by Wadsley [16]. The crystal structure has been determined as a double layer structure in which each layer is composed of double zigzag ribbons of octahedra sharing corners with an orthorhombic symmetry, a space group *Pnma* and lattice parameters of $a = 6.46$ Å, $b = 3.79$ Å, $c = 18.47$ Å. Compared to layered silicate clays, crystalline $KTiNbO_5$ has a well-defined structure in an atomic scale. It allows obtaining particles with a high degree of purity, leading to an easier characterization of the layers by X-ray diffraction and a greater regularity of the hybrid structures. Indeed, earlier publications have demonstrated the possibility of inserting long-chain amines in the oxide interlayer space [17–22].

In this study, from $KTiNbO_5$, inorganic–organic hybrids were synthesized to make polyethylene nanocomposites. For this task, *N*-alkyl amines with varying alkyl chain lengths have been used to increase the interlayer space, modify the oxide surface and make easier the compatibility between the polymer and the inorganic nanofiller. These materials have been then incorporated into a polyethylene matrix by melt processing. The influence of these hybrid nanofillers has been investigated through many characterizations: X-ray diffraction to pattern the different steps of the nanocomposite synthesis, mechanical and rheological tests by static and dynamic measurements, related to morphologies of the nanocomposites determined by scanning and transmission electron microscopies. Finally differential scanning calorimetry and thermogravimetric analyses have been performed to evaluate the thermal behavior of the nanocomposites.

2. Experimental section

2.1. Materials

Titanium oxide (Prolabo), niobium oxide (Prolabo) and potassium carbonate (Prolabo) were used to synthesize $KTiNbO_5$.

Tetradecylamine (TDA) (Fluka), hexadecylamine (HDA) (Aldrich) and octadecylamine (ODA) (Aldrich) were used to modify layered titanoniobate oxide $HTiNbO_5$.

Nanocomposites have been processed with linear low density polyethylene (Flexirene® MR50), furnished by Polimeri Europa.

2.2. Synthesis

2.2.1. Preparation of $KTiNbO_5$ and $HTiNbO_5$

$KTiNbO_5$ ($M = 259.8$ g mol^{-1}) was prepared by solid state reaction between TiO_2, Nb_2O_5 and K_2CO_3 with a molar ratio of (2:1:1), respectively. The precursors were first mixed and preheated at 600 °C. After grinding, the platinum crucible containing the powders was placed in a tubular furnace at 1200 °C with a temperature ramp of 3°/min to avoid the formation of parasite condensed phases [23,24]. The protonic oxide $HTiNbO_5$ was obtained by ion exchange in 6 N hydrochloric acid on $KTiNbO_5$ and stirred for about 3 days at room temperature.

2.2.2. Intercalation of N-alkyl amines

The method consists in a reversible acido-basic reaction between $HTiNbO_5$ (10^{-2} mol L^{-1}) and the amine in ethanol/water (75/25 by volume) solvent for 24 h at 60 °C. To increase the intercalation probability an excess of amine (1.5 eq./$HTiNbO_5$) was used during the reaction. The separation of the solid hybrid from the solvent was performed by filtration and the white crystalline solid was washed several times with a 60 °C ethanol/water (75/25 by volume) solvent to remove all the non-intercalated amine. Finally, the powder was dried at 100 °C for 8 h. The samples are named: C_{14}HTi, C_{16}HTi and C_{18}HTi according to the carbon chain length of the intercalated amine.

2.2.3. Preparation of the hybrid nanocomposites

Hybrid nanocomposites were obtained by melt intercalation of modified nanoparticles in polyethylene (2% and 5% by weight) using a twin screw 15 cc DSM microcompounder. The mixture was sheared for about 1 min at 100 rpm at 190 °C and injected with a 10 cc moulding device at 30 °C to obtain dumbbell-shaped specimens. The samples are named: PE, PE–KTi, PE–HTi, PE–C_{14}, PE–C_{16} and PE–C_{18} according to the filler incorporated.

2.3. Characterization

X-ray diffraction (XRD) measurements were performed using copper target tube (Cu Kα radiation, $\lambda = 1.5406$ Å) equipping powder diffractometers: a D8 BRUKER and an X'Pert Philips, respectively, fitted with a capillary geometry by transmission mode for low 2θ measurements and a classical sample holder. The microstructure of modified oxides and the dispersion of the nanofillers in polyethylene were investigated by scanning electron microscopy (SEM) using a Zeiss supra 55 electron microscope and by transmission electron microscopy using a JEOL 2010 FEG STEM operated at 200 kV. Energy dispersive spectroscopic (EDS) analyses were done with EDAX Si/Li detectors fitted on both microscopes.

Nanocomposite specimens for electron microscopic observations were prepared by cutting slices of the filled polymer at low temperature (in liquid nitrogen). For SEM studies, these slices were first directly observed using very low beam conditions (under 5 kV) and then coated with a thin carbon layer before EDS analyses. For TEM studies, thin slices of filled polymer were chosen and placed between two 0.8 mm aperture Ni grids on the sample holder and the thinnest parts (near the edge of the slice) were then observed and analysed by EDS using STEM technique.

Phase transitions were determined on a Perkin–Elmer DSC 7 differential scanning calorimeter at 20 °C/min under nitrogen (20 mL/min) and calibrated in temperature and heat flow with indium.

Thermal degradation of the modified oxides and nanocomposites was performed using a Perkin–Elmer TGA 7 under nitrogen gas flow (20 mL/min).

Dynamical mechanical analysis (DMA) characterizations were carried out with a controlled stress rheometer (TA AR1000) in rectangular torsion mode. A frequency of 1 Hz and a temperature sweep between −60 °C and 140 °C in the linear viscoelastic domain were chosen for the analysis.

For tensile tests, an IR30 K with 2.5 kN cell Lloyd test machine was used at room temperature. They were performed on the injected dumbbell-shaped specimens (width 4 mm × thickness 2 mm × length of parallel part 25 mm × total length 75 mm).

3. Results and discussion

The purity of pristine oxide $KTiNbO_5$ was confirmed by X-ray powder diffraction and the diffractogram was analysed using the Pattern Matching mode of Fullprof program [25] with space group and cell parameters according to Ref. [16]. The calculated pattern fits with the experimental one and all diffraction peaks are indexed in the $KTiNbO_5$ lattice ($a = 6.44$ Å, $b = 3.80$ Å and $c = 18.41$ Å) and *Pnma* space group. As shown in Fig. 1a, no extra peaks are observed in the pattern.

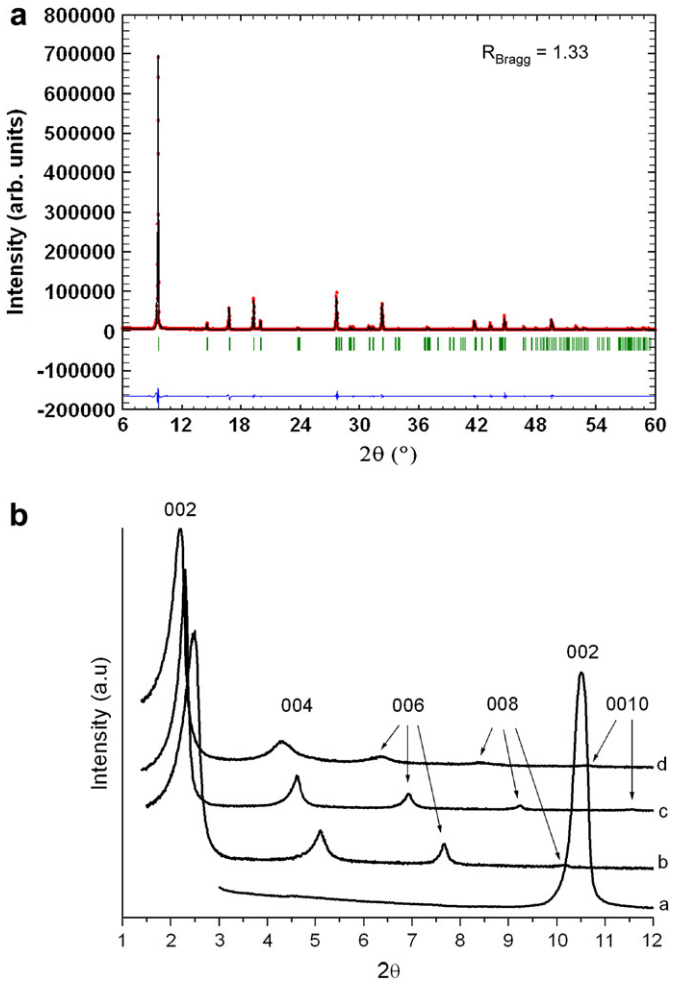

Fig. 1. (a) Observed (dots), calculated (lines) and difference XRPD patterns of $KTiNbO_5$ refined in pattern matching mode. Vertical bars indicate the position of the reflexions of $KTiNbO_5$, (b) X-ray diffraction powder patterns of (a) $HTiNbO_5$, (b) $C_{14}HTi$, (c) $C_{16}HTi$, and (d) $C_{18}HTi$.

3.1. Intercalation of $HTiNbO_5$ by N-alkyl amines

The modified titanoniobate oxides have been characterized by X-ray diffraction. The low angle XRD diagrams ($1.3 < 2\theta < 12°$) of $HTiNbO_5$ ((a) in Fig. 1b) present a single peak corresponding to the 002 reflection as calculated from the orthorhombic lattice parameter and the space group *Pnma* ($a = 6.53$ Å, $b = 3.78$ Å, $c = 16.68$ Å) according to Ref. [26]. Indeed in that case, reflections: $0kl$ with $k + l \neq 2n$; $hk0$ with $h \neq 2n$; $h00$, $0k0$, $00l$ with h, k, and $l \neq 2n$ are systematically absent and therefore no 001 peak can be observed. However, d_{002} ($=c/2$) is proportional to the interlayer spacing. It will allow calculating the interlayer spacing via the d_{002} value. It can be noted as well that narrow and well-resolved peaks, with several diffraction orders show the well-organized structure of the modified $HTiNbO_5$, which is not the case with modified clays. The average calculation of FWHM confirms this fact. For comparison the FWHM of the 002 reflexions of the $C_{18}HTi$ and a montmorillonite modified by octadecylamine [27] has been measured. The FWHM values are, respectively, close to 0.11° and 0.28°. These values confirm the relatively well-crystallized structure of the hybrids.

Fig. 2 shows the linear dependence of the c parameter as a function of alkyl chain length. The theoretical alkyl chain length can be calculated as [17]

$$L_c\,(\mathrm{A}) = 1.257 \times (n_C - 1) + 3.9 \quad (1)$$

Here the C−C bonds are supposed to be in all-*trans* conformation including the polar head and $n_C - 1$ is the number of methylene group. The size of the methyl group at the end of the alkyl chain and the polar head is equal to 3.9 Å.

The experimental c parameter dependence versus L_c is

$$c = 2.5 \times L_c + 16.9 \quad (2)$$

The maximum value is obtained for ODA with *ac* parameter of 81 Å which is almost five times that of $HTiNbO_5$.

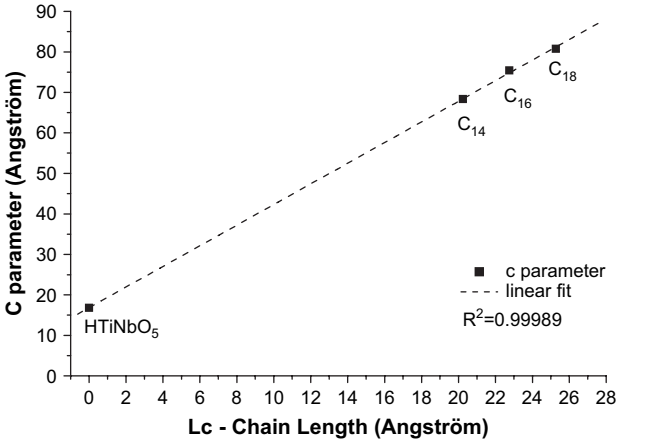

Fig. 2. Linear dependency of the lattice parameter c as a function of amine chain length (L_c).

Lambert et al. [17] have examined several models to explain the orientation of the alkyl chains in the $HTiNbO_5$ interlayer space. Indeed, it strongly confirms that the *N*-alkyl chains are oriented as a bilayer without overlapping and more or less tilted because of a slope superior to 2 (2). It is then possible to evaluate the tilt angle α respective to the mineral layer as

$$\sin(\alpha) = \left(d_{002} - \frac{8.3}{2}\right) \Big/ L_c \quad (3)$$

In this equation, d_{002} is the interlayer distance calculated from XRD diagrams and 8.3/2 is the d_{002} of the pristine $HTiNbO_5$. A tilt angle close to 40° is obtained regardless of the amine intercalated.

Elemental analyses of the modified oxides have been carried out to evaluate the formula and to know the mole number of amine inserted respective to number of available sites. The measurements have been done on nitrogen, carbon and hydrogen, but the most accurate and repeatable is for carbon. They are given in Table 1. These results allow relating to the cation exchange capacity (CEC) of the material, which gives a CEC three times higher than the montmorillonite CEC [28].

We have got higher results compared to those reported by Kikkawa and Koizumi [18] mentioning an amount of intercalated compound of 50%. The difference may be due to the use of an excess of amine [27].

In order to confirm the elemental analysis results, thermogravimetric analyses have been performed on the same hybrid materials and $HTiNbO_5$ (see Fig. 3). Previous investigations by Xie et al. [29] reported that the thermal decomposition of organic substances between silicate layers was mainly in the range 200–500 °C. These authors proposed that the organic modifiers start decomposing at temperature around 200 °C as our hybrids, and that the small molecular weight organics are released first, while the high molecular weight organic species are released at higher temperature because they might be trapped by the montmorillonite interspaces. The studies show that the decomposition product was a mixture of alkanes, alkenes and primary amines according a Hofmann elimination or nucleophile substitution 2 (SN_2). Thermal decomposition of organic molecules predominately occurs at the site with the smallest bond dissociation energy. The bond energies within alkyl amines decrease in the order C–H (96–99 kcal/mol), N–H (93 kcal/mol), C–C (83–85 kcal/mol), and C–N (69–75 kcal/mol) [30].

Our studies reveal that the organo-modified titanoniobates are stable up to 200 °C which makes them good potential fillers for polymers that are processed at lower temperatures.

Table 1
Elemental analysis and CEC for modified oxides

	%C (±0.1)	Mole per formula unit (±0.01)	CEC (eq./100 g)
$HTiNbO_5 + NH_2C_{14}H_{29}$	30.4	0.65	293
$HTiNbO_5 + NH_2C_{16}H_{33}$	34.7	0.71	320
$HTiNbO_5 + NH_2C_{18}H_{37}$	35.2	0.64	289

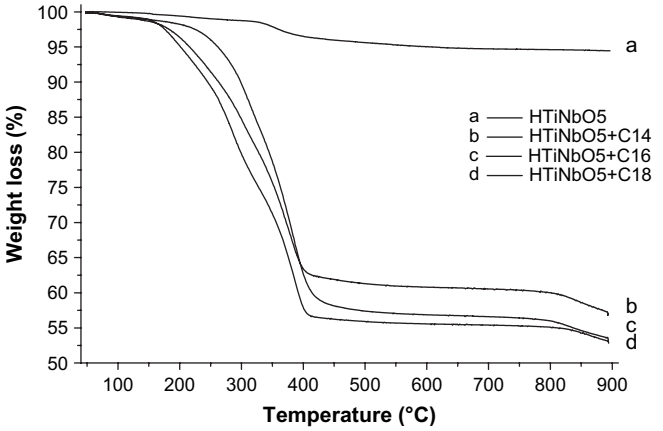

Fig. 3. Weight loss of $HTiNbO_5$ and modified oxides.

The weight loss between 50 °C and 110 °C can be attributed to the absorbed water.

The weight loss during decomposition between 110 °C and 800 °C allows evaluating the quantity of organic moieties in the hybrids. For the $C_{14}HTi$, $C_{16}HTi$ and $C_{18}HTi$ hybrids, the percentage of inserted molecule is 58%, 65% and 56%, respectively. The quantities degraded up to 800 °C are slightly lower than the one obtained in microanalysis. However, making the hypothesis that only the alkyl chain is calcinated by a Hofmann decomposition process and that the ammonium group remains at the oxide surface beyond 800 °C, it gives an amine insertion percentage of 67%, 73% and 62%, respectively. These last results are more in agreement with the elemental analysis results from Table 1.

Therefore, it is possible to explain why the maximum of inserted amines is not reached. Indeed, the surface area of $HTiNbO_5$ is 24.5 $Å^2$/charge. Supposing that alkyl chains have the same conformation of polyethylene chains (zigzag in orthorhombic cell, space group *Pnam* and lattice parameter at 23 °C: $a = 7.41$ Å, $b = 4.95$ Å and $c = 2.55$ Å), the minimum distance between two chains is 4.46 Å which would lead to a surface of 19.9 $Å^2$ in a square lattice. We have seen above that alkyl chains are tilted with a tilt angle of 40°; their projection gives a projected surface of 30.96 $Å^2$. In that case, the maximal substitution ratio would be $\rho_{max} = 0.8$ which is the theoretical maximal value of insertion ratio.

The morphology of the pristine oxide $KTiNbO_5$ and the acidic form $HTiNbO_5$ modified with amines by acido-basic reaction has been observed by SEM. From Fig. 4a it was found that the raw material $KTiNbO_5$ has a compact layered structure. But after the insertion of amine (b), a splitting of the layers is observed. It shows that the intercalation process has been successfully achieved and will help layers' exfoliation when dispersed in polyethylene.

3.2. Characterization of the nanocomposites

Fig. 5 presents XRD powder patterns of polyethylene filled with the different hybrid materials. The measurements have been performed on cryo grinded test specimens. The

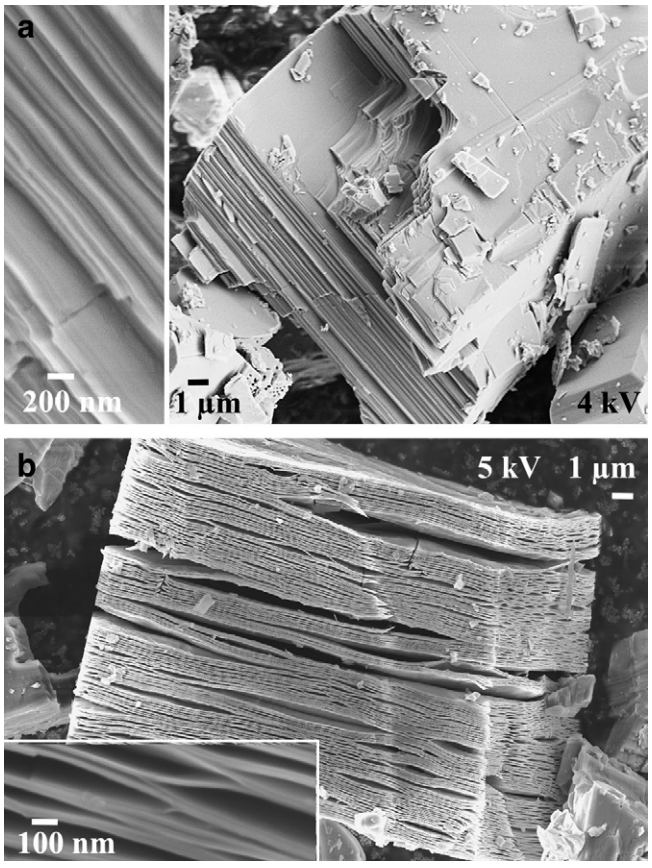

Fig. 4. SEM images of (a) $KTiNbO_5$ and (b) $C_{18}HTi$ (inset: enlargements of each image).

polyethylene pattern (a) shows two peaks corresponding to the d_{110} and d_{200} in the orthorhombic system, as expected. PE–KTi (b) and PE–HTi (c) patterns show the 002 characteristic peak from the interlayer space of the mineral oxide. This demonstrates that the layers are still well organized and that no delamination has occurred. In the same way, the PE–C_{14}, PE–C_{16}, PE–C_{18}, respectively, (d)–(f) patterns, exhibit low intensity peaks in the small angle region. They correspond to the same harmonics shown in Fig. 1. It points out that the

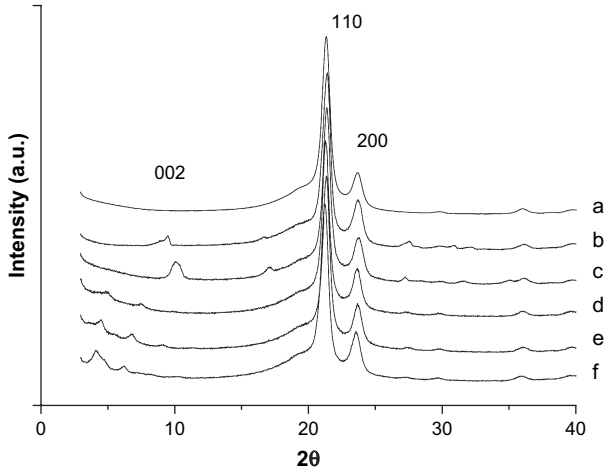

Fig. 5. X-ray diffraction powder patterns of (a) polyethylene (PE), (b) PE–KTi, (c) PE–HTi, (d) PE–C_{14}, (e) PE–C_{16} and (f) PE–C_{18}.

hybrid material is not fully delaminated in the polyethylene matrix. This can be due to the extreme non-polarity of the polymer.

In order to complete our XRD study on the characterization of the layered hybrids exfoliation and dispersion in the polymer matrix in micro- and nanoscale, SEM and TEM studies have been undertaken.

We have investigated two types of samples. These two samples, respectively, considered as references for polyethylene filled by non-exfoliated and exfoliated titanoniobates, are the samples PE–KTi 5% (i.e. PE + 5%$KTiNbO_5$) and PE–C18 5% (i.e. PE + 5% of modified $HTiNbO_5$ by octadecylamine).

The SEM image obtained with the integrated annular AsB (Angle selective Backscattered electron) detector presented in Fig. 6a reveals the heterogeneous morphology of PE–KTi 5%, since big aggregates are clearly visible in the polymer matrix at low magnification. The EDS analysis shows that these aggregates contain K, Ti, Nb cations. On an enlargement (Fig. 6b), the morphology of the aggregate incorporated in the polymer can be directly compared to the initial morphology, compact layered structure, of the raw material, $KTiNbO_5$ as shown in Fig. 4a. It confirms that there is no exfoliation of the non-compatibilized titanoniobates in the polyethylene matrix.

On the observations of PE–C18 5% (SEM image in Fig. 7 and EDS mapping of the sample in Fig. 8), the difference between our two reference samples is obvious. In both the figures the major part of the titanoniobate is present in the sample in the shape of small thin plates (less than 1 µm wide) pointed by white arrows in Fig. 7 and statistically distributed in the polymer matrix. Another important fact can be deduced from these observations. Some aggregates of poorly exfoliated

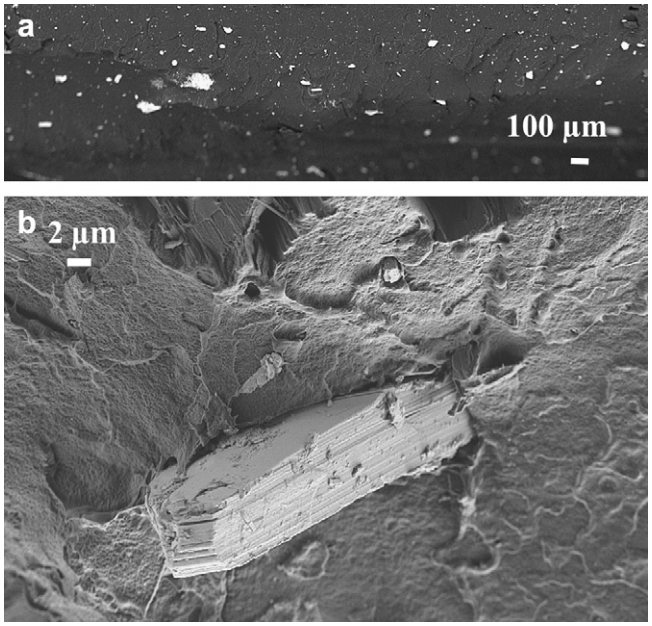

Fig. 6. (a) SEM image of PE–KTi 5%, $KTiNbO_5$ appears as white in PE matrix and (b) enlargement of the image showing the compact layered structure of a $KTiNbO_5$ aggregate (non-exfoliated material) inserted in the polymer matrix.

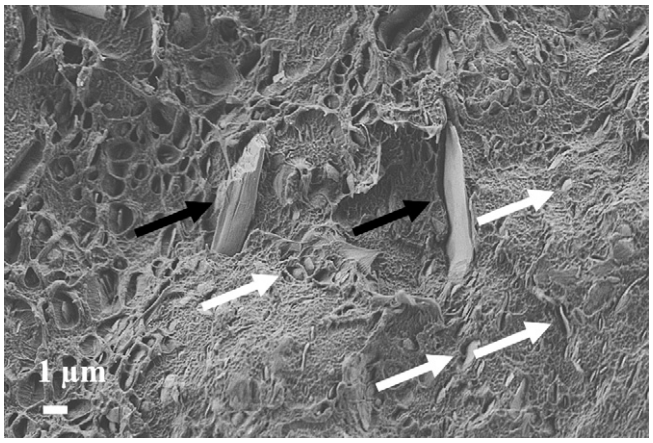

Fig. 7. SEM image of PE−C_{18} 5%; small tactoids of titanoniobate are pointed by white arrows while black arrows point out aggregates with a compact layered structure (non-exfoliated).

hybrid materials are still present in that sample (see black arrows in Fig. 7). These aggregates are responsible for the persistence of small diffraction peaks at very low angle in XRD patterns. These two phenomena are in good agreement with the XRD study.

TEM observations performed on individual thin slices of nanocomposite coupled with EDS mapping using the STEM option of the TEM confirmed all these points. The material presents a strong lamellar morphology with particles ranging from a few sheets (for example see Fig. 9) to numbered thicker particles made of several sheets. Fig. 10 shows the edge of

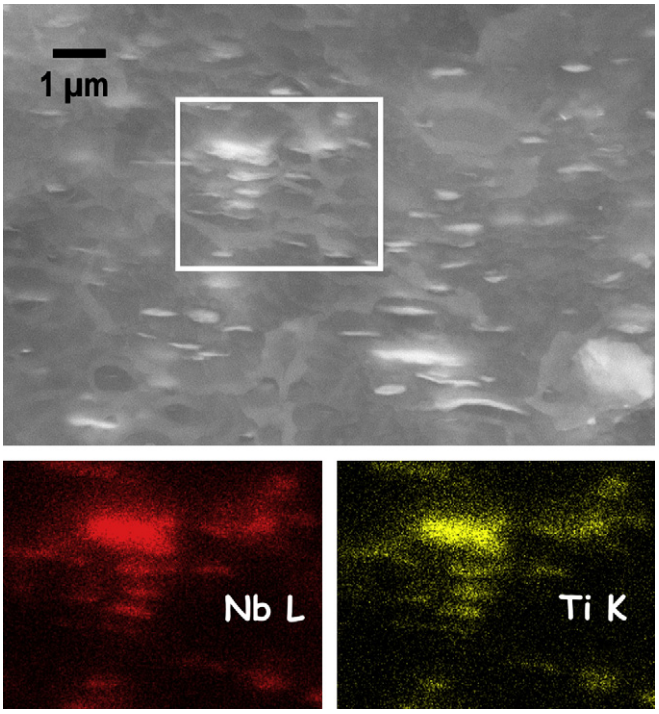

Fig. 8. Top: SEM image with AsB detector of PE−C_{18} 5% showing that the hybrid material is statistically distributed in the polymer matrix. Bottom: EDS mapping of the selected area showing that Ti and Nb atoms are strictly located in the particle of hybrid material.

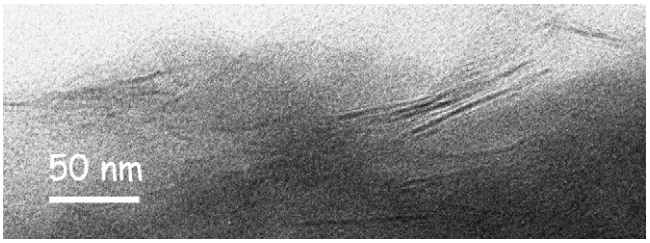

Fig. 9. HREM image of the PE−C_{18} 5% nanocomposite showing single sheet or groups of exfoliated sheets dispersed in the polymer matrix.

a distorted plate where the stacking of few sheets (<10) forming the small plates imaged by SEM (Fig. 7, white arrows) is clearly evidenced.

Fig. 11 presents the TEM image and the associated EDS mapping of a small tactoid on the edge of our observed sample. The polymer is imaged by the carbon map while the Ti, Nb and O maps show that these atoms are strictly located in the plate and have not diffused in the PE matrix, i.e. the modified titanoniobate oxide plate has not been deteriorated by the exfoliation in the polymer matrix.

The weight loss of the nanocomposites at 5% is plotted as a function of temperature (Fig. 12). It can be firstly noticed that all the nanocomposites have a degradation temperature higher than that of the pure polyethylene. For all of them, the degradation occurs in one step, supposing the good homogeneity of the final material. Furthermore, a difference between nanocomposites based on non-modified oxides and those with hybrids can be seen. The interest of adding a surfactant is demonstrated.

The evolution of the end degradation temperature for the different composites at two different filling rates is plotted in Fig. 13. It is obvious that the filling rate is related to the composite's thermal stability.

The analysis is the same when the *N*-alkyl amine chain is longer. It demonstrates that PE nanocomposites have better thermal stability than pure PE. It can be noticed that incorporation of $HTiNbO_5$ does not improve the thermal stability

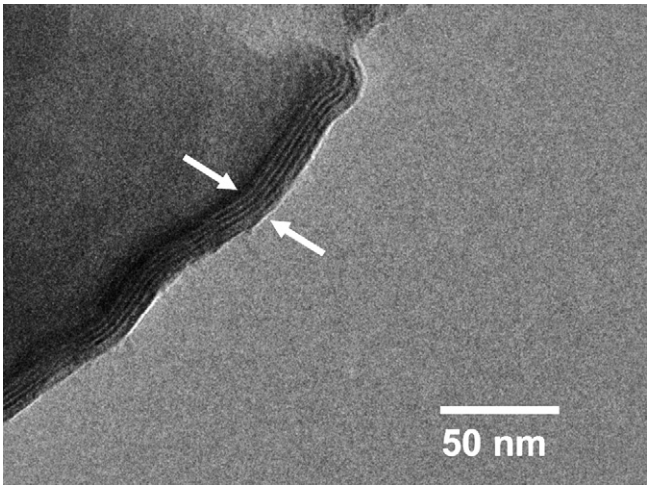

Fig. 10. HREM image of a distorted titanoniobate stacking with few exfoliated sheets forming the single particle.

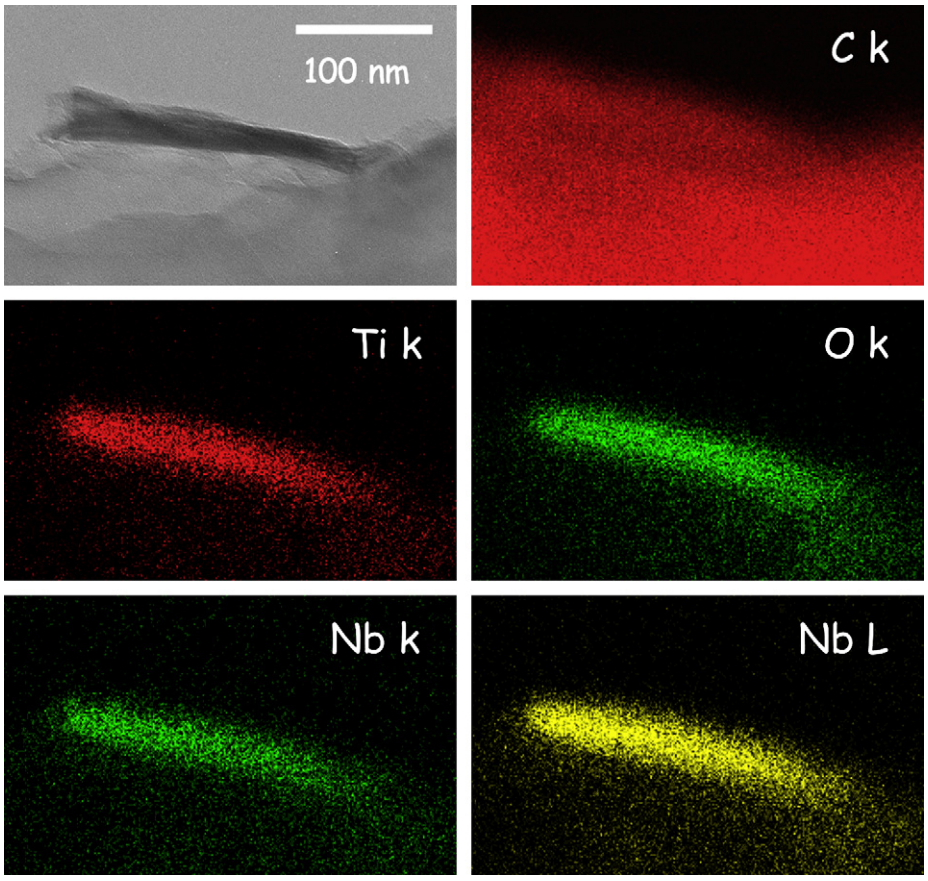

Fig. 11. STEM image and EDS mapping of an individual thin oxide plate. The modified titanoniobate has not been deteriorated by the exfoliation process.

compared to incorporation of $KTiNbO_5$. Moreover, slight increase when extending the chain length might indicate an effect of the better exfoliation despite the lack of full delamination.

DSC measurements on the nanocomposites between −20 °C and 160 °C reveal no shift of the melting peak at around 120 °C and no further transition. The enthalpies given in Table 2 are slightly the same. It suggests that the insertion of hybrid nanofillers does not modify significantly the crystallinity of the material compared to the polymer matrix. This will allow comparing directly the mechanical properties and link them strictly to the filler dispersion and not to change the matrix properties.

The dynamic mechanical properties are obtained from controlled stress rheometer measurements. Fig. 14 shows the storage (G') modulus values of PE nanocomposites. The storage modulus of all the nanocomposites is higher than pure PE.

In order to characterize the thermomechanical stability of the composites, the inset in Fig. 14 presents the temperature

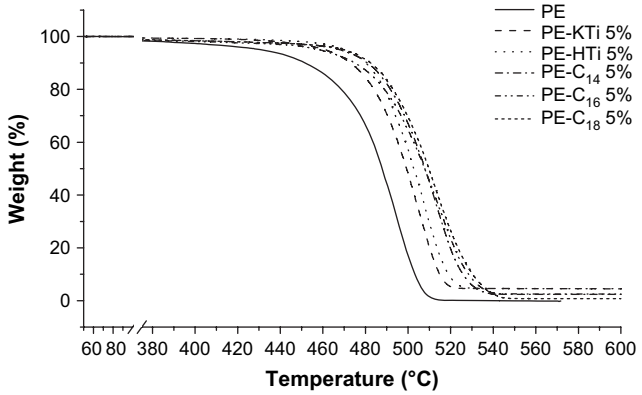

Fig. 12. Thermogravimetric analysis of the nanocomposites.

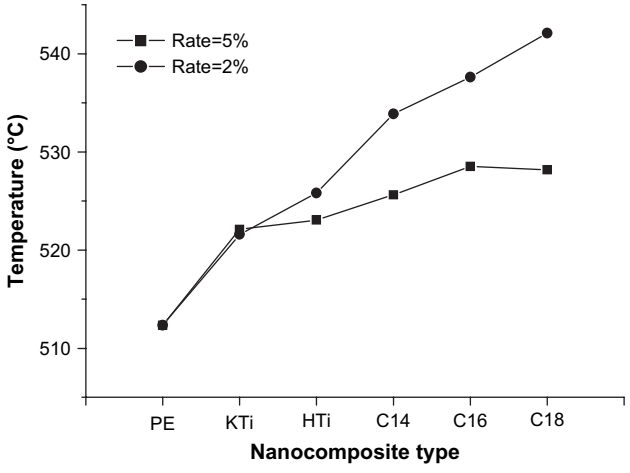

Fig. 13. Evolution of the end degradation temperature for the different nanocomposites at 2% and 5%.

Table 2
Enthalpies and percentage of crystallinity of the PE nanocomposites

Nanocomposite at 5%	ΔH (J/g) (±1)	% Crystallinity (±1)
PE	132	46
PE + $KTiNbO_5$	136	47
PE + $HTiNbO_5$	134	46
PE + C_{14}	138	48
PE + C_{16}	136	47
PE + C_{18}	137	47

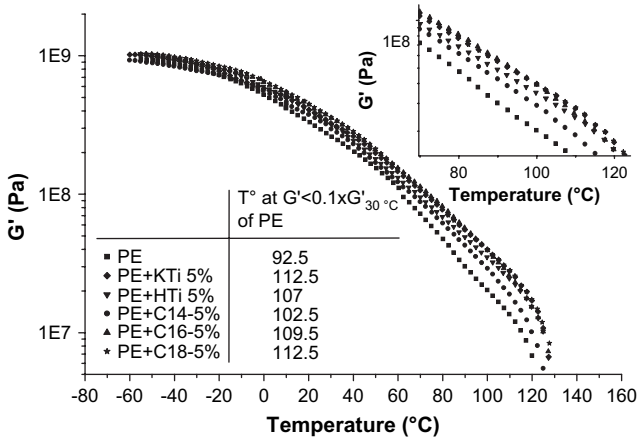

Fig. 14. Dynamic modulus G' as a function of temperature, for polyethylene and hybrid nanocomposites at 5% (inset: temperature of the PE nanocomposites at $G' < 0.1 \times G'_{30\ °C\ \text{of PE}}$).

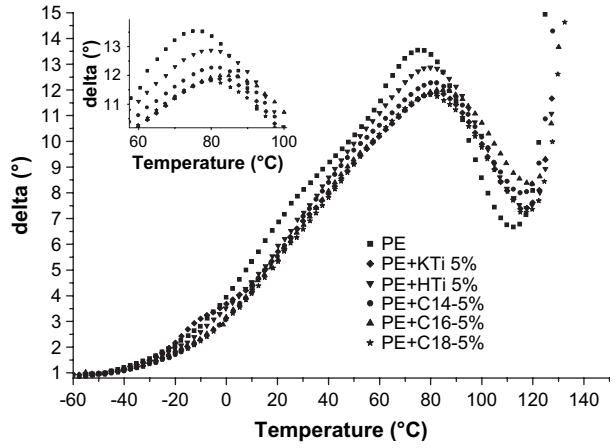

Fig. 15. Delta as a function of temperature, for polyethylene and hybrid nanocomposites at 5%.

at which the composite storage modulus reaches 10% of the modulus of neat PE at 30 °C. Thermomechanical stability is improved for all nanocomposites when compared to unfilled PE. Surprisingly, the thermomechanical stability is improved at the same level when using unmodified $KTiNbO_5$ or C18HTi as nanofiller. It seems that titanoniobates exfoliation thanks to amine intercalation is not the only parameter to impact this property. However, the hybrid nanocomposites show a linear increase of their softening temperature as a function of chain length, which confirms the improvement due to better exfoliation.

At −60 °C, G' is close to the glassy modulus. It decreases continuously up to the melting without well-marked glass transition. However, the delta damping angle in Fig. 15 presents a maximum at around 80 °C attesting a mechanical relaxation. This maximum shifts to higher temperatures for the nanocomposites and its magnitude is reduced. This suggests that the energy dissipation process is slowed down by the nanofillers. It means that the interactions between the polymer matrix and the nanofillers are stronger and therefore the macromolecules' mobility decreases. This is due to the exfoliation and the high shape factor of the nanofillers.

The tensile test results for the nanocomposites at 2% and 5% of filling rate are presented in Table 3. It can be pointed out that the tensile modulus increases especially for the nanocomposite with the *C*18-hybrid at 5%, while the elongation at break decreases strongly. The maximum strength follows the same trend mostly at 5%. Nevertheless, the yield strength does not change significantly. These results correlate the dynamical results, claiming that the presence of inorganic or hybrid structures hinders the molecular mobility in the nanocomposite leading to a more brittle material.

Surprisingly, the results for the PE + $KTiNbO_5$ nanocomposite, i.e. non-modified oxide, are close to those with *C*18-hybrid. The same observation has been done for the dynamical mechanical tests as well. This phenomenon might be explained by the fact that volume fraction of inorganic compound in $KTiNbO_5$ is superior to that of the *C*18-hybrid. However, when we compare the $KTiNbO_5$ and $HTiNbO_5$ nanocomposite results, they are highly different, though their inorganic volume fractions are equivalent. It could deal with a difference of hydrophilia between the pristine $KTiNbO_5$ and the acidic oxide $HTiNbO_5$. The latter might be more hydrophilic, so less compatible with the hydrophobic polyethylene matrix.

Table 3
Tensile test results for nanocomposites at 2% and 5% filling rates

Composite	Young's modulus (MPa) (±71 MPa)		Yield strength (MPa) (±0.6 MPa)		Max strength (MPa) (±1.3 MPa)		Elongation at break (±0.8)	
	2 wt%	5 wt%	2 wt%	5 wt%	2 wt%	5 wt%	2 wt%	5 wt%
PE	259		15.3		21.5		8.5	
PE + $KTiNbO_5$	302	331	15.2	15.3	17.0	16.5	6.0	6.0
PE + $HTiNbO_5$	267	312	15.0	15.3	21.7	19.6	9.0	7.6
PE + C_{14}	265	294	15.7	15.9	22.0	18.0	9.4	7.4
PE + C_{16}	286	301	15.9	16.4	21.6	14.9	9.1	5.4
PE + C_{18}	308	350	15.7	15.9	21.5	14.0	9.5	4.7

4. Conclusion

Nanostructured organic/inorganic hybrid materials based on the modification of the titanoniobate oxide $KTiNbO_5$ by *N*-alkyl amines have been successfully prepared. X-ray diffraction and scanning electron microscopy have showed the increase of the interlayered space. The *N*-alkyl chains adopt a double layer tilted without overlapping arrangement. Nanocomposites containing pristine $KTiNbO_5$ and several hybrid nanofillers with different alkyl chain lengths have been prepared by polyethylene melt intercalation. The thermomechanical property analysis of the nanocomposites reveals an increase of Young's modulus of 35%, the degradation temperature is 20 °C higher than the neat polyethylene while the elongation at break decreases by half. The morphologies have been investigated by SEM, TEM coupled with EDS mapping representing the dispersion and the degree of exfoliation of the filler. It has been revealed that the modification of the oxide improves the state of dispersion and the exfoliation of the nanoparticles. These observation techniques are an interesting mean of characterization for further nanocomposite studies.

Acknowledgments

The authors would like to acknowledge Emmanuel Guilmeau for his help in the collection of the SEM images and EDS mapping characterization, and Nicolas Barrier for his help in the collection of low angle XRD patterns.

References

[1] Okada A, Kawasumi O, Usuki A, Kojima Y, Kurauchi T, Kamigaito O. Mater Res Soc Symp Proc 1990;171.
[2] Usuki A, Kojima Y, Kawasumi O, Okada A, Fukushima T, Kurauchi T, et al. J Mater Res 1993;8.
[3] Kojima Y, Usuki A, Kawasumi O, Okada A, Kurauchi T, Kamigaito O. J Polym Sci Part A Polym Chem 1993;31:983–6.
[4] Kojima Y, Usuki A, Kawasumi O, Okada A, Kurauchi T, Kamigaito O. J Polym Sci Part A Polym Chem 1993;31:1755–8.
[5] Okada A, Usuki A. Mater Sci Eng C Biomim Mater Sens Syst 1995;3:109–15.
[6] Powell CE, Beall GW. Curr Opin Solid State Mater 2006;10:73–80.
[7] Sue H-J, Gam KT. Chem Mater 2004;16:242–9.
[8] Tjong SC. Mater Sci Eng R 2006;53:73–197.
[9] Chrissopoulou K, Altintzi I, Anastasiadis SH, Giannelis EP, Pitsikalis M, Hadjichristidis N, et al. Polymer 2005;46:12440–51.
[10] Vermogen A, Masenelli-Varlot K, Séguéla R. Macromolecules 2005;38:9661–9.
[11] Tanniru M, Yuan Q, Misra RDK. Polymer 2006;47:2133–46.
[12] Ma D. J Polym Sci Part B Polym Phys 2005;43:488–97.
[13] Lee G-W, Park M, Kim J, Lee JI, Yoon HG. Scr Mater 2006;55:1119–22.
[14] Bruzaud S, Beigbeider A, Médéric P, Aubry T, Grohens Y. Polymer 2005;46:12279–86.
[15] Bruzaud S, Levesque G. Chem Mater 2002;14:2421–6.
[16] Wadsley AD. Acta Crystallogr 1964;17:623.
[17] Lambert JF, Deng Z, D'Espinose JB, Fripat JJ. J Colloid Interface Sci 1989;132.
[18] Kikkawa S, Koizumi M. Mater Res Bull 1980;15:533–9.
[19] Tagaya H, Saito K, Kuwahara T, Kadokawa J, Chiba K. Catal Today 1993;16:463–70.
[20] Rebbah H, Borel MM, Raveau B. Mater Res Bull 1980;15:317.
[21] Rebbah H, Borel MM, Bernard M, Raveau B. Rev Chim Miner 1981;18:109.
[22] Lagaly G. Solid State Ionics 1986;22:43–51.
[23] Rebbah A, Desgardin G, Raveau B. J Solid State Chem 1980;31:321–8.
[24] Colin J-F, Pralong V, Caignaert V, Hervieu M, Raveau B. Inorg Chem 2006;45:18.
[25] Rodriguez-Carvajal J. Program Fullprof 2000; 2001.
[26] Rebbah A, Pannetier J, Raveau B. J Solid State Chem 1982;41:57–62.
[27] Le Pluart L, Duchet J, Sautereau H, Gerard J-F. J Adhes 2002;78:645–62.
[28] Bergaya F, Vayer M. Appl Clay Sci 1997;12:275–80.
[29] Xie W, Gao Z, Liu K, Pan W-P, Vaia R, Hunter D, et al. Thermochim Acta 2001;339:367.
[30] Xie W, Gao ZM, Pan WP, Hunter D, Singh A, Vaia RA. Chem Mater 2001;13:2979.